Wavelength conversion and supercontinuum generation in silicon optical fibers

Anna C. Peacock, *Senior Member, IEEE,* Joseph Campling, Antoine F. J. Runge, Haonan Ren, Ozan Aktas, Peter Horak, Noel Healy, Ursula J. Gibson, and John Ballato, *Fellow, IEEE*

(Invited Paper)

Abstract—This paper describes the state-of-the-art in wavelength conversion and supercontinuum generation using glass-clad silicon core optical fibers. Such semiconductor fibers have enjoyed considerable attention due to their intrinsically high third-order nonlinearities, which are markedly higher than conventional infrared glasses. Results to-date from small core silicon fibers fabricated using both the high pressure chemical vapor deposition (HPCVD) and the molten core drawing (MCD) method are presented. Also discussed are directions for continued study and development including improved interconnection and alloys with stronger nonlinearities? [anything else??].

Index Terms—IEEE, IEEEtran, journal, LaTeX, paper, template.

1 Introduction

Since their realization a decade ago, glass-clad, semiconductor core optical fibers have received considerable attention globally as potential alternatives to soft-glasses for infrared and nonlinear fiber optics [1]. Of the semiconductors fabricated into fibers to-date, silicon is by far the most studied and advanced with performance in fiber-form now rivaling, if not exceeding, that in planar analogs. While transmission losses still need to be further reduced, preferably by an order of magnitude, and smaller core sizes achieved, the high third-order susceptibility of the silicon core material mark these fibers as particularly interesting for infrared sources based on wavelength conversion and supercontinuum generation.

This paper reviews progress in the studies of nonlinear propagation in the silicon core fibers. It begins with a brief discussion of the two methods employed to fabricate silicon optical fiber; including their relative advantages and disadvantages. From there, the nonlinear model used to describe light in the silicon fibers is described, followed by experiments and numerical simulations to investigate wavelength conversion in fibers with amorphous and (poly)crystalline silicon core materials. Lastly, opportunities for future study to improve the efficiency of these fibers for nonlinear systems are provided.

A. C. Peacock, J. Campling, A. F. J. Runge, H. Ren, O. Aktas, and Peter Horak are with the Optoelectronics Research Centre, University of Southampton, Southampton, SO17 1BJ, UK (e-mail: acp@orc.soton.ac.uk).
N. Healy is with Newcastle University.
U. Gibson is with the Department of Physics, Norwegian University of Science and Technology, 7491 Trondheim, Norway.
J. Ballato is with the Center for Optical Materials Science and Engineering Technologies (COMSET) and Department of Materials Science and Engineering, Clemson University, Clemson, SC 29634, USA.
Manuscript received April 19, 2005; revised August 26, 2015.

2 Silicon Fiber Fabrication

Fabricating optical fibers out of crystalline or amorphous semiconductors poses a significant challenge in materials science due to their thermal, chemical, and mechanical mismatch with traditional glass fiber materials. For example, many semiconductors have melting points that are not in the same temperature range as the glass transition of fused silica, and/or do not melt congruently [2]. However, over the past 10 years two practical approaches to fabricating semiconductor optical fibers have emerged, the high pressure chemical vapor deposition (HPCVD) technique [3] and the molten core drawing (MCD) process [4]. Both methods have their advantages and disadvantages, for example the HPCVD technique can be used to produce fibers with both amorphous and crystalline silicon cores, but is limited to fiber lengths of a few meters. Alternatively, the MCD process has so far been restricted to crystalline cores, but can be used to produce kilometers of fiber. Thus the techniques are very much complementary, as outlined below.

2.1 High Pressure Chemical Vapor Deposition

The first demonstration of a silicon core fiber was produced by depositing the semiconductor material into the central pore of a silica capillary using the HPCVD method [5]. In this process, the capillary tubes have the dual function of acting as a reaction chamber for the deposition and as the low refractive index cladding material required for waveguiding. Prior to deposition, the silane precursor is mixed with a carrier gas to promote molecular transport though the capillary. The reaction is thermally initiated at the required location and, as the precursors decompose, the material is conformally deposited onto the capillary walls until the core is filled. Fig. 1(a) shows a scanning electron microscope (SEM) image of a silicon fiber fabricated via this approach, confirming that the core consists of a solid silicon rod. Owing to the extremely smooth surfaces of the capillary templates (roughness values $\sigma \sim 0.1\,\mathrm{nm}$ [6]) the core/cladding interface is near atomically smooth, which

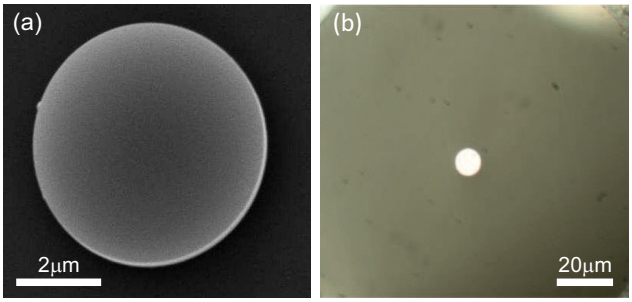

Fig. 1. Silicon core fibers fabricated via (a) the HPCVD approach and (b) the MCD method.

is particularly important for reducing scattering associated with the high index contrast, and thus achieving low loss waveguides [7].

A key advantage of the HPCVD method is that the temperatures and pressures can be controlled to fill capillary dimensions ranging from several tens of micrometers down to much smaller, hundreds of nanometers, dimensions that are favoured for nonlinear applications. Furthermore, as the energy for precursor decomposition is significantly lower than that required for melting the bulk material, it can be undertaken at relatively low temperatures, which reduces cracking and defect formation associated with the thermal mismatch of the materials [8]. However, significant disadvantages of this approach are that, owing to the small core sizes, the deposition rate is slow and it is difficult to control the grain growth when depositing in a crystalline form [9].

2.2 Molten Core Drawing

The MCD technique is based on a modified fiber drawing method, whereby the silica cladding acts as a crucible to contain the silicon as it is melted and drawn down to form the fiber core [10]. Owing to the practicality of the fiber drawing method, it is this approach that has been the most widely adopted by the fiber fabrication community [4], [11], [12]. Typically, the fibers are drawn from a preform consisting of a silica tube filled with pure silicon, which can be in the form of a solid rod or powder. The preform is then heated to above both the glass transition temperature of the cladding and the melting temperature of the core. At this temperature the cladding glass can be deformed, but is still viscous enough to contain the molten silicon and maintain its cylindrical geometry when drawn. As the fiber leaves the furnace, it rapidly cools and the liquid core solidifies into a polycrystalline form, which is surrounded by the silica cladding. Fig. 1(b) displays a microscope image of a MCD derived silicon fiber, where the high index core is clearly visible with a well-defined core/cladding interface.

Key benefits of the MCD technique are that it can produce very long lengths of fiber and, by selecting the appropriate draw conditions, fibers with cores that consist of long (almost centimeter length) single crystal grains can be produced with relatively low optical losses [13], [14]. The main drawbacks of this method are associated with the high draw temperatures that are needed to soften the cladding, which can cause oxygen to diffuse into the core and induce significant cracking as the different materials cool. Although these issues can be somewhat mitigated via the introduction of a diffusion barrier around the core Ref. [12], as of to date, silicon core fibers fabricated from this method have been limited to core sizes that are several microns in diameter, or larger. Clearly the ability to obtain smaller core sizes is highly desirable for nonlinear applications and is thus work in this area is ongoing.

3 Nonlinear Propagation in Silicon Fibers

As silicon is a uniform symmetric material, nonlinear transmission in these fibers is governed by processes involving the third order $\chi^{(3)}$ nonlinearity. The real part of $\chi^{(3)}$ gives rise to the Kerr nonlinear refractive index n_2 and the imaginary part to the two photon absorption (TPA) parameter β_{TPA}. Thus pulse propagation in the silicon core fibers can be described by a modified form of the nonlinear Schrödinger equation (NLSE) [15]:

$$\begin{aligned}\frac{\partial A(z,t)}{\partial z} &= -\frac{i\beta_2}{2}\frac{\partial^2 A(z,t)}{\partial t^2} + i\gamma\left|A(z,t)\right|^2 A(z,t) \\ &- \frac{1}{2}\left(\sigma_f + \alpha_l\right) A(z,t), \end{aligned} \quad (1)$$

where $A(z,t)$ is the pulse envelope, β_2 is the group velocity dispersion (GVD) parameter, γ is the nonlinearity parameter, α_l is the linear loss, and σ_f defines the free carrier contributions. Here, the nonlinear parameter is complex to account for both the Kerr and TPA contributions: $\gamma = k_0 n_2/A_{\mathrm{eff}} + i\beta_{\mathrm{TPA}}/2A_{\mathrm{eff}}$, where A_{eff} is the mode area. Similarly, the free carrier term is also complex $\sigma_f = \sigma\left(1 + i\mu\right)N_c$, where σ is the free carrier absorption (FCA) coefficient and μ governs the free carrier dispersion (FCD), and depends on the free carrier density N_c. The carrier density is related to the TPA parameter and can be determined via the rate equation [15]:

$$\frac{\partial N_c\left(z,t\right)}{\partial t} = \frac{\beta_{\mathrm{TPA}}}{2h\nu_0}\frac{\left|A\left(z,t\right)\right|^4}{A_{\mathrm{eff}}^2} - \frac{N_c\left(z,t\right)}{\tau_c}, \quad (2)$$

where τ_c is the carrier lifetime.

Compared to silica fibers, the silicon core material has a large nonlinearity and a high refractive index, which results in tight mode confinement, so that the nonlinear effects can be enhanced by several orders of magnitude [16]. As a result, propagation in the silicon fibers requires much lower pump powers (watts compared to kilowatts) and shorter fiber lengths (centimeters compared to kilometers) to observe efficient nonlinear wavelength conversion. However, the precise requirements will depend on the nature of the silicon material and how it has been produced, which can alter both the linear and nonlinear parameters, as well as the fiber core size.

4 HPCVD Amorphous Silicon Fibers

The first observations of nonlinear propagation in silicon core fibers were recorded in a hydrogenated amorphous core material [17]. This is because, compared to crystalline silicon, hydrogenated amorphous silicon (a-Si:H) has a high Kerr nonlinear coefficient, on the order of $2-5$ times larger, as well as low linear and nonlinear optical losses [18]. The precise values for the linear and nonlinear properties

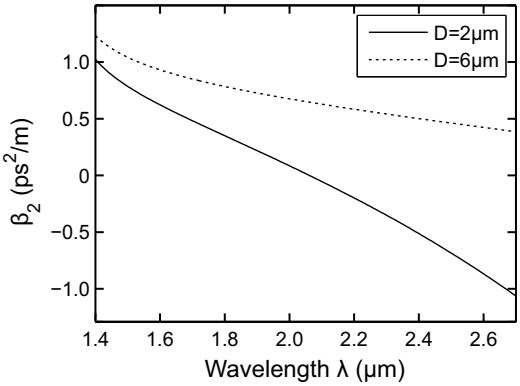

Fig. 2. Group velocity dispersion curves for two silicon fibers with micron-sized core diameters (see legend).

of this material depend on the hydrogen content, which can be controlled through the deposition parameters such as the precursor mixture and the temperature, as well as the operating wavelength. Typical parameter ranges for the HPCVD fibers fabricated from this material are shown in Table 2 for two pump wavelengths of interest; one in the telecoms band and one in the mid-infrared [19]. We note that these values are very similar to what has been reported for a-Si:H waveguides on-chip, indicating that the material quality is comparable [20].

TABLE 1
Material parameters for a-Si:H core fibers.

Pump λ	$1.55\,\mu$m	$2.4\,\mu$m
α_l (dB/cm)	0.9-3.5	0.5-2
n_2 ($\times 10^{-13}$ cm^2/W)	1.5-1.85	1.0-1.3
β_{TPA} (cm/GW)	0.5-0.8	0.01-0.03

As all of the initial nonlinear investigations of these fibers were conducted in structures with fairly large $\sim 6\,\mu$m core diameters, where the dispersion properties are dominated by the large normal material dispersion (see Fig. 2), the observed spectral broadening was fairly modest [17]. Nevertheless, it was still possible to use these fibers for all-optical processes such as ultrafast modulation [21] and switching [22]. However, a significant breakthrough was made when low loss a-Si:H fibers with much smaller, $\sim 1-2\,\mu$m, core diameters were produced [23]. In this regard, reducing the core size had a two fold advantage; firstly, the nonlinearity was enhanced via the reduction in the mode area, and secondly, the increased waveguide dispersion could compensate for the material dispersion to access the anomalous dispersion regime, as illustrated in Fig. 2. As a result, these small core fibers opened a route for the observation of nonlinear processes such as four-wave mixing (FWM) and soliton effects that are critical for generating broadband supercontinuum.

To demonstrate this, a a-Si:H fiber with a $1.7\,\mu$m diameter core was pumped with a high power, femtosecond ($T_{\mathrm{FWHM}} \sim 300$ fs), optical parametric oscillator (OPO) to investigate the process of spontaneous FWM. By tuning the OPO to operate on the edge of the anomalous dispersion regime ($\lambda_p = 2.28\,\mu$m), where optimum efficiency for the phase-matched process is expected, the characteristic FWM sidebands appeared on either side of the pump (see inset in Fig. 3(a)). In this region, the phase-matching condition can be well approximated by [24]:

$$\beta_2\Omega^2 + 2\mathrm{Re}[\gamma]\mathrm{P}_0 = 0, \tag{3}$$

where P_0 is the peak pump power and $\Omega = |\omega_p - \omega_s| = |\omega_p - \omega_i|$ is the frequency shift between the pump and the signal/idler. Thus the position of the peak FWM gain can be estimated as $\Omega_{\max} = \pm\sqrt{2\mathrm{Re}[\gamma]\mathrm{P}_0/|\beta_2|}$. Fig. 3 shows the measured tunability of the FWM peaks as a function of (a) pump power and (b) pump wavelength in comparison to the predicted phase-matching curves, showing very good agreement. Furthermore, the results in Fig. 3(b) indicate that with only 20 W peak power it is possible to tune the wavelength conversion over 600 nm (2 μm to 2.6 μm), while only tuning the pump by 280 nm. By increasing the pump power to ~ 60 W, this could increase to ~ 900 nm.

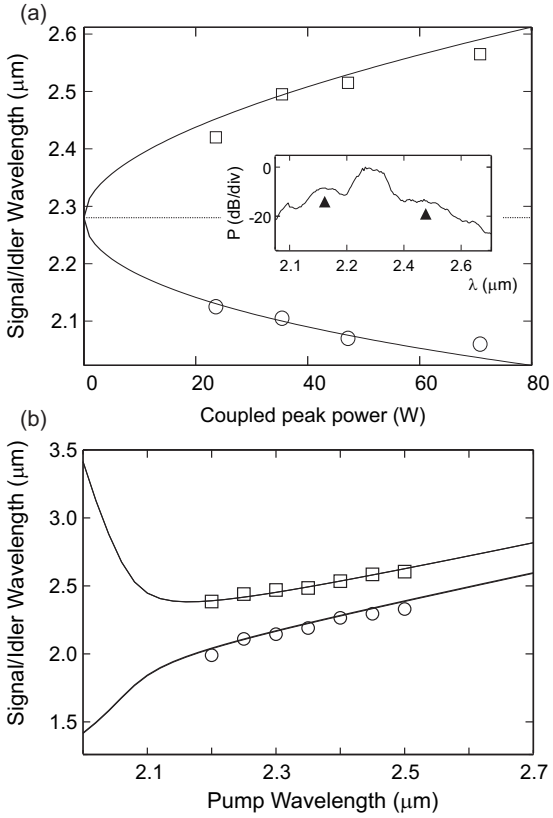

Fig. 3. (a) Peak FWM signal (circles) and idler (squares) wavelengths plotted as a function of coupled peak power for $\lambda_p = 2.28\,\mu$m. Inset shows a typical spectrum with the FWM sidebands indicated by up-arrows. (b) FWM signal (circles) and idler (squares) positions as a function of pump wavelength for $P_0 = 20$ W. In both cases the solid lines are the phase-matching predictions from $\Omega_{\max}$.

By increasing the pump power even further, the FWM process can be used to seed supercontinuum generation. Fig. 4 shows the spectral broadening obtained for various pump wavelengths with a launch power of 75 W. The top spectrum corresponds to the same pump wavelength as Fig. 3(a), however, in this case the generated spectral bandwidth is much broader (by ~ 500 nm). The shape of this spectrum suggests that the increased broadening is due to the appearance of a second set of sidebands positioned

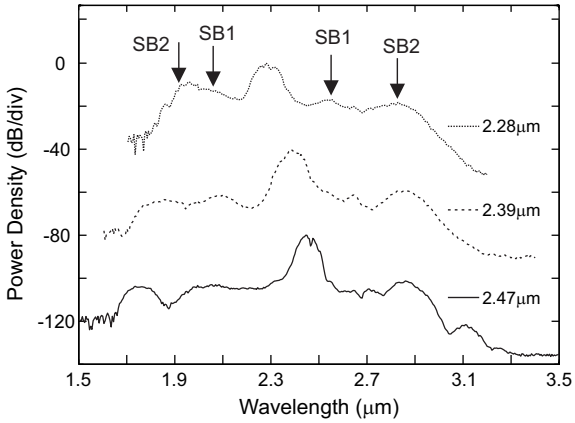

Fig. 4. Supercontinuum spectra generated in a a-Si:H core fiber pumped in the anomalous dispersion regime with $P_0 = 75\,\mathrm{W}$ and central wavelengths as labeled. The arrows indicate the positions of the 1st and 2nd order FWM sidebands (SB1 and SB2).

at $2\Omega_{\max}$, associated with a higher order FWM process (see arrows). We attribute the ability to phase-match cascaded FWM processes to the high nonlinearity of the fiber that facilitates wavelength conversion over short propagation lengths, in this case a $4\,\mathrm{mm}$ long fiber. The remaining spectra in Fig. 4 have been obtained for increasingly longer pump wavelengths, where the linear and nonlinear losses are lower. In all cases these spectra exhibit more than an octave of continuum generation at the $30\,\mathrm{dB}$ level, with the total spectral coverage extending from $1.64\,\mu\mathrm{m}$ to $3.37\,\mu\mathrm{m}$ ($\sim 1700\,\mathrm{nm}$). Interestingly, as well as an increase in the spectral bandwidth, the bottom two spectra exhibit an additional feature on the short wavelength edge characteristic of dispersive wave emission. Although dispersive waves are often associated with the onset of soliton fission, as the length of our fiber is shorter than the estimated fission length for the input pulses ($L_{\mathrm{fiss}} \simeq L_{\mathrm{D}}/N \sim 7\,\mathrm{mm}$, where $L_D = T_0^2/|\beta_2| \sim 5\,\mathrm{cm}$ is the dispersion length and $N \sim 8$ is the soliton order), we attribute their appearance here to temporal break-up of the pulses caused by FWM induced modulation [25]. Further verification of this process is provided by the good agreement between the position of these short wavelength peaks centered at $\sim 1.8\,\mu\mathrm{m}$ and the predicted wavelength of the dispersive wave emission $\lambda_{\mathrm{DW}} \sim 1.75\,\mu\mathrm{m}$ as calculated via the phase-matching condition in Ref. [26].

To gain more insight into the underlying dynamics driving the supercontinuum generation in this material, numerical simulations based on a modified version of Eqs. (1) and (2) were performed, which also included third order dispersion, Raman scattering and self steepening terms [25]. The simulated waveguide parameters were similar to the ones experimentally measured in Ref. [23]. We set the linear loss to be $\alpha_l = 0.8\,\mathrm{dB/cm}$, nonlinear refractive index $n_2 = 1.04 \times 10^{-13}\,\mathrm{cm^2/W}$, carrier lifetime $\tau_c = 87\,\mathrm{ns}$, $\beta_{\mathrm{TPA}} = 0.02\,\mathrm{cm^2/GW}$, and $A_{\mathrm{eff}} = 1.23\,\mu\mathrm{m}^2$. The dispersion parameters $\beta_2 = -0.59\,\mathrm{ps^2/m}$ and $\beta_3 = 5.6 \times 10^{-3}\,\mathrm{ps^3/m}$ were calculated from the Sellmeier equation for crystalline silicon and raising it by $\sim 4\,\%$ to account for the higher refractive index of a-Si:H. Fig. 5(a) shows the simulated supercontinuum spectrum at the output of a $4\,\mathrm{mm}$ length of a-Si:H fiber for input pulses of $180\,\mathrm{fs}$ FWHM and $75\,\mathrm{W}$ input power centered at $2.47\,\mu\mathrm{m}$. The corresponding temporal and spectral evolution of the pulse propagating in the a-Si:H fiber are shown in Fig. 5(b) and (c), respectively.

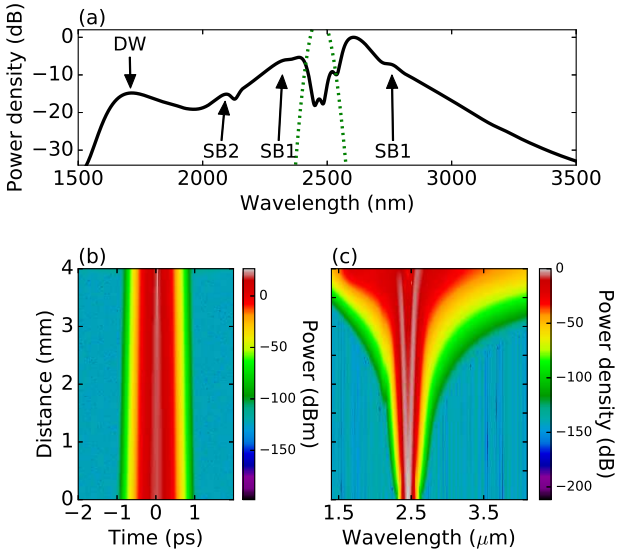

Fig. 5. (a) Simulated supercontinuum spectrum generated in a a-Si:H core fiber pumped at $2.47\,\mu\mathrm{m}$ with $75\,\mathrm{W}$ input peak power (black) and input pulse spectrum (dashed green). Temporal (b) and spectral (c) evolution of the optical pulses in the a-Si:H fiber.

The numerical results of Fig. 5(a) are in reasonable agreement with the experimental spectrum in Fig. 4, in terms of the $-30\,\mathrm{dB}$ bandwidth ($1822\,\mathrm{nm}$ compared to $1700\,\mathrm{nm}$ in the experiment) and the appearance of several peaks around the pump wavelength. The first sidebands (SB1) appear at 2.32 and $2.76\,\mu\mathrm{m}$, close to both the theoretical predictions and experimental spectrum. In addition, a second sideband (SB2) is clearly visible at $2.09\,\mu\mathrm{m}$ and a dispersive wave is generated around $1.71\,\mu\mathrm{m}$, again matching the experimental observations and thus providing further confirmation of the dynamics described above. The temporal and spectral evolution of the pulse, shown in Fig. 5(b) and (c), indicate that most of the spectral broadening occurs after $3\,\mathrm{mm}$ of fiber. As seen in Fig. 5(b), the pulse becomes narrows before splitting into two via FWM-induced modulation after $3.85\,\mathrm{mm}$ of propagation. The first pulse peaks at $3.94\,\mathrm{mm}$ before transferring further energy to the second, leading to the emission of the dispersive wave. We also note that the soliton fission lengths for the other pump wavelengths are significantly longer, which yields narrower broadening, as also seen in Fig. 4.

5 MCD Polysilicon Fibers

Compared to the a-Si:H fibers, studies of nonlinear propagation in the p-Si MCD fibers have been much more limited. This is due both to the larger core sizes of the as-drawn MCD fibers, where typical diameters are tens to hundreds of microns [4], [12], as well as the higher losses associated with scattering and absorption at the grain boundaries in the polycrystalline material [14]. To address these issues, a novel tapering procedure has been developed to post-process the as-drawn fibers [27]. As well as reducing the core size of

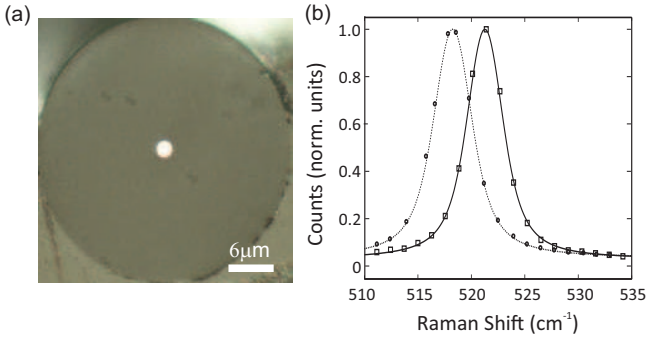

Fig. 6. (a) Microscope image of a tapered p-Si core fiber with a core diameter of $\sim 2\,\mu$m. (b) Raman spectra of the p-Si core (circles) compared to a single crystal wafer.

the fibers, the procedure also acts to improve the overall crystallinity of the core by enhancing the grain growth and aligning the crystal orientation with respect to the fiber axis [28]. The values for the linear and nonlinear properties of this material will thus depend on the averaged crystallinity, where we expect the key parameters to approach those of single crystal materials in the fibers with the largest grain sizes, i.e., when the volume of amorphous and defect material is at a minimum.

Using this tapering procedure, a number of low loss ($\sim 1-4\,\mathrm{dB/cm}$) p-Si fibers have been demonstrated with core sizes in the range $900\,\mathrm{nm}-4\,\mu$m [27], [29]. Fig. 6(a) shows a microscope image of a tapered p-Si fiber with a core diameter of $\sim 2\,\mu$m and Fig. 6(b) shows the corresponding Raman spectrum, as compared to a single crystal reference. The slight downshifting in the position of fiber Raman peak is due to residual strain associated with differences in the thermal expansion of the core/cladding materials. Nevertheless, the excellent agreement in the Raman widths ($2.9\,\mathrm{cm}^{-1}$ for the fiber compared to $2.7\,\mathrm{cm}^{-1}$ of the reference) indicates that the core is composed of large grain p-Si.

To demonstrate the suitability of these fibers for nonlinear propagation a set of high power transmission measurements were conducted, with the goal to benchmarking the values of the nonlinear refractive index and TPA parameter. As TPA manifests as an intensity dependent absorption, β_{TPA} can be determined simply by monitoring the output power as a function of the coupled input power, as shown in Fig. 7(a). Subsequently, the size of n_2 can be estimated by mapping the spectral broadening due to self-phase modulation (SPM), shown in Fig. 7(b). In both cases the experimental data was obtained using a fiber with a core diameter of $D = 2\,\mu$m and a linear loss value of $\alpha_l \sim 2\,\mathrm{dB/cm}$, which was pumped with a high power $1.54\,\mu$m soliton source ($T_{\mathrm{FWHM}} \sim 700$ fs). The numerical fits were calculated using Eqs. (1) and (2), with the remaining material parameters estimated from the single crystal values [15]. The results yield best fit values of $\beta_{\mathrm{TPA}} \sim 0.7\,\mathrm{cm/GW}$ and $n_2 \sim 0.5\times10^{-14}\,\mathrm{cm}^2/\mathrm{W}$, which are both within the range previously reported for single crystal silicon [30]. Table 7 summarizes the key linear and nonlinear parameters measured in a selection of tapered MCD p-Si fibers with the lowest losses, which we expect to consist of the largest crystal grains. Significantly, these measurements represent the first reports of nonlinear propagation in a p-Si waveguide, either fiber or planar-based, which we attribute to the high material quality of the post-processed fibers.

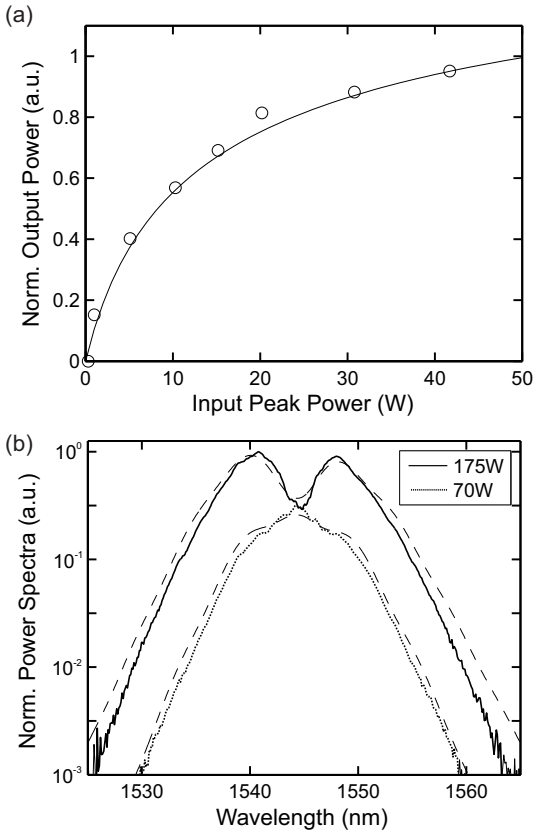

Fig. 7. (a) Spectral broadening as a function of coupled peak power for two input powers (see legend). The dashed curves are simulated fits to estimate n_2.(b) Nonlinear absorption as a function of coupled input peak power. The solid curve is the simulated fit to estimate β_{TPA}.

TABLE 2
Material parameters for tapered p-Si core fibers.

Pump λ	$1.55\,\mu$m
α_l (dB/cm)	1.6-3
n_2 ($\times10^{-14}$ cm^2/W)	4-6
β_{TPA} (cm/GW)	0.7-1.0

As these first characterization measurements were performed in the telecoms band where the material dispersion is normal, observations of FWM and/or broadband continuum generation have yet to be made in these fibers. However, as key benefit of the MCD fibers is their long lengths, we have been able to fabricate p-Si tapers with micrometer sized cores over lengths of $\sim 2-3\,\mathrm{cm}$, which is considerably longer than the few millimeter lengths more typical of the HPCVD fibers [23]. Thus, in order to compare the suitability of these fibers for supercontinuum generation against the HPCVD fibers, numerical investigations similar to those of Fig. 5 have been performed. The fiber parameters were based on a tapered p-Si structure with a $2\,\mu$m core diameter and length of $13\,\mathrm{mm}$. With the pump pulses positioned at $2.42\,\mu$m, we can assume: $\alpha \sim 1\,\mathrm{dB/cm}$, $n_2 = 5.15\times10^{-14}\,\mathrm{cm}^2/\mathrm{W}$, $\tau_c = 87\,\mathrm{ns}$, $\beta_{\mathrm{TPA}} = 0.02\,\mathrm{cm}^2/\mathrm{GW}$, $A_{\mathrm{eff}} = 1.68\,\mu\mathrm{m}^2$ and the calculated dispersion parameters of $\beta_2 = -0.23\,\mathrm{ps}^2/\mathrm{m}$ and $\beta_3 = 4\times10^{-3}\,\mathrm{ps}^3/\mathrm{m}$.

The simulation results are shown in Fig 8. Similar to the deposited fiber, the spectral broadening is dominated

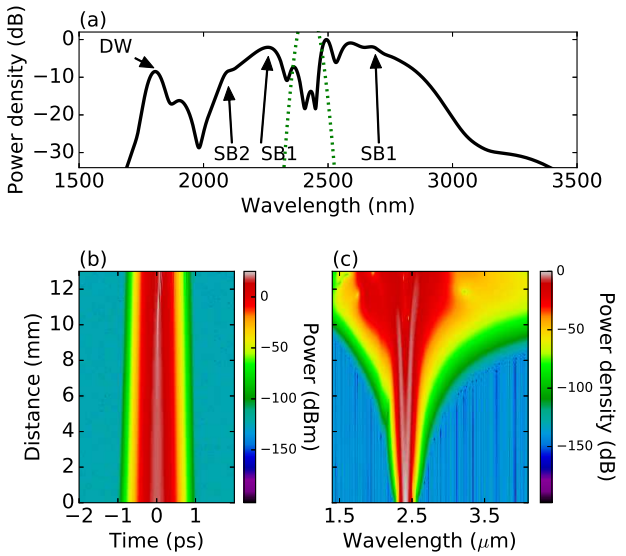

Fig. 8. (a) Simulated supercontinuum spectrum generated in a p-Si core fiber pumped at $2.42\,\mu\mathrm{m}$ with $75\,\mathrm{W}$ input power (black) and input pulse spectrum (dashed green). Temporal (b) and spectral (c) evolution of the optical pulses in the p-si fiber.

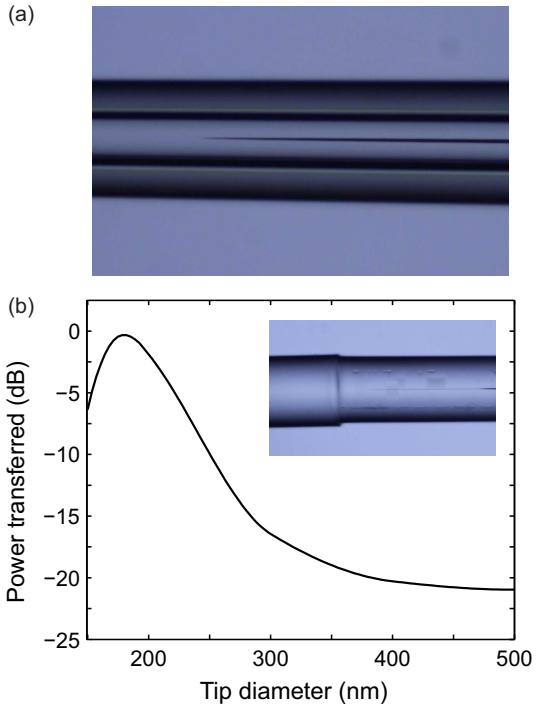

Fig. 9. (a) Microscope image of a silicon nano-spike for efficient input coupling. (b) Mode overlap between the silicon nano-spike and a standard SMF as a function of tip diameter. Inset shows the spliced SMF-silicon nano-spike device.

by cascaded FWM. The first sidebands (SB1) are calculated to occur at $2.2\,\mu\mathrm{m}$ and $2.66\,\mu\mathrm{m}$ and appear at $2.26\,\mu\mathrm{m}$ and $2.69\,\mu\mathrm{m}$, respectively. The second sidebands (SB2) are predicted $2.04\,\mu\mathrm{m}$ and $2.96\,\mu\mathrm{m}$. As in the previous case, only the short wavelength SB2 is observable at $2.1\,\mu\mathrm{m}$, in good agreement with the theory. As expected, a first dispersive wave is emitted at $1.95\,\mu\mathrm{m}$, but not until $11\,\mathrm{mm}$ of propagation owing to the lower nonlinear index of this material. The dispersive wave does, however, shift out further to $1.8\,\mu\mathrm{m}$ at the end of the fiber, resulting in a $-30\,\mathrm{dB}$ spectral bandwidth of $1460\,\mathrm{nm}$. Although this broadening is below what was obtained in the a-Si:H fiber, and less than an octave, it could be increased quite significantly by reducing the losses and increasing the taper lengths as this would allow for propagation beyond the soliton fission length. Experimental efforts in this area are currently ongoing.

6 Future Challenges

6.1 Interconnection

Despite their physical similarity to SMFs, coupling light efficiently into and out of the silicon core fibers remains a difficult task due to silicon's high refractive index, which results in significant reflection losses and a large mode mismatch. A few solutions have been proposed to overcome this integration challenge, including the use of microstructured fiber designs to better match the mode area [31] and chemical etchants to reduce the reflection at the interface [32], though so far no method has addressed both issues simultaneous. Thus a promising alternative solution would be to adapt the well-established inverse taper approach widely employed by the planar community [33], which is also gaining attention within the novel material fiber community [34]. The key idea behind this approach is that by decreasing the silicon core to nanoscale dimensions at the facet, the guided mode spreads out to better match both the area and the effective index of the SMF mode.

To demonstrate this, the tapering procedure described in Section 5 has been adapted to fabricate nano-spikes on the end of the high quality p-Si fibers as shown in Fig. 9(a) [35]. These spikes can be cleaved and spliced to standard SMF, using a modified fusion splicing technique, to obtain a robust join (see inset in Fig. 9(b)). Optical transmission measurements of the integrated silicon fiber-SMF device have revealed insertion losses of $\sim 7\,\mathrm{dB}$. Although a promising preliminary result, the relatively high losses of this system can be attributed to non-optimized dimensions of the nano-spike and a slight misalignment of the spliced fiber cores. Indeed, numerical simulations of the mode overlap at the splice joint calculated as a function of the tip diameter, as shown in Fig. 9(b), indicate that the maximum transmission between the two fibers could reach as high as $\sim 0.5\,\mathrm{dB}$ for an optimized tip diameter of $190\,\mathrm{nm}$. Clearly, such low integration losses would greatly improve the efficiency and practicality of the nonlinear systems.

7 Conclusion

This paper has reported the recent advances in wavelength conversion and supercontinuum generation in silicon optical fibers. We first discussed the various types of silicon fibers through the different fabrication techniques that have been developed over the past decade. For both deposited and molten silicon fibers, the key achievement has been the significant reduction of the linear optical loss that allows for nonlinear effects to be generated. In a-Si:H fiber, we have demonstrated octave spanning supercontinuum by pumping close to the ZDW, around $2\,\mu\mathrm{m}$. Numerical simulations, in reasonable agreement with the experimental

results, revealed that the spectral broadening is indeed dominated by cascaded FWM. Our recent work on molten silicon fibers allows us to fabricate waveguides with core diameters that are small enough to reach the anomalous dispersion regime at similar pumping wavelengths. Numerical simulations show promising results for the generation of supercontinuum in polycrystalline material fibers. Finally, our derived tapering technique paves the way for the full integration of the devices in an all-fiber system. We believe that this work highlights the great potential of this platform for the efficient generation of complex nonlinear dynamics over the near-infrared and the mid-infrared spectral region.

ACKNOWLEDGMENT

The authors would like to thank...

REFERENCES

[1] A. C. Peacock, U. J. Gibson, and J. Ballato, "Silicon optical fibres - past, present, and future," *Advances in Physics: X*, vol. 1, p. 114, 2016.
[2] S. Morris, T. Hawkins, P. Foy, J. Ballato, S. W. Martin, and R. Rice, "Cladding glass development for semiconductor core optical fibres," *Int. J. Appl. Glass. Sci.*, vol. 3, p. 144, 2012.
[3] L. Lagonigro, N. Healy, J. R. Sparks, N. F. Baril, P. J. A. Sazio, J. V. Badding, and A. C. Peacock, "Low loss silicon fibers for photonic applications," *Appl. Phys. Lett.*, vol. 96, p. 041105, 2010.
[4] J. Ballato, T. Hawkins, P. Foy, R. Stolen, B. Kokuoz, M. Ellison, C. McMillen, J. Reppert, A. M. Rao, M. Daw, S. Sharma, R. Shori, O. Stafsudd, R. R. Rice, and D. R. Powers, "Silicon optical fiber," *Opt. Express*, vol. 16, p. 18675, 2008.
[5] P. J. A. Sazio, A. Amezcua-Correa, C. E. Finlayson, J. R. Hayes, T. J. Scheidemantel, N. F. Baril, B. R. Jackson, D.-J. Won, F. Zhang, E. R. Margine, V. Gopalan, V. H. Crespi, and J. V. Badding, "Microstructured optical fibers as high-pressure microfluidic reactors," *Science*, vol. 311, p. 1583, 2006.
[6] P. J. Roberts, F. Couny, H. Sabert, B. J. Mangan, D. P. Williams, L. Farr, M. W. Mason, A. Tomlinson, T. A. Birks, J. C. Knight, and P. S. J. Russell, "Ultimate low loss of hollow-core photonic crystal fibres," *Opt. Express*, vol. 13, p. 236, 2005.
[7] N. Healy, L. Lagonigro, J. R. Sparks, S. Boden, P. J. A. Sazio, J. V. Badding, and A. C. Peacock, "Polycrystalline silicon optical fibers with atomically smooth surfaces," *Opt. Lett.*, vol. 36, p. 2480, 2011.
[8] N. F. Baril, R. He, T. D. Day, J. R. Sparks, B. Keshavarzi, M. Krishnamurthi, A. Borhan, V. Gopalan, A. C. Peacock, N. Healy, P. J. A. Sazio, and J. V. Badding, "Low loss silicon fibers for photonic applications," *J. Am. Chem. Soc.*, vol. 134, p. 19, 2011.
[9] S. Chaudhuri, J. R. Sparks, X. Ji, M. Krishnamurthi, L. Shen, N. Healy, A. C. Peacock, V. Gopalan, and J. V. Badding, "Crystalline silicon optical fibers with low optical loss," *ACS Photonics*, vol. 3, p. 378384, 2016.
[10] J. Ballato and E. Snitzer, "Fabrication of fibers with high rare-earth concentrations for faraday isolator applications," *Appl. Opt.*, vol. 34, p. 6848, 1995.
[11] B. Scott, W. Ke, and G. Pickrell, "Fabrication of n-type silicon optical fibers," *Photon. Technol. Lett.*, vol. 21, p. 1798, 2009.
[12] E. Nordstrand, A. Dibbs, A. Eraker, and U. J. Gibson, "Alkaline oxide interface modifiers for silicon fiber production," *Opt. Mater. Express*, vol. 3, p. 651, 2013.
[13] J. Ballato, T. Hawkins, P. Foy, S. Morris, N. K. Hon, B. Jalali, and R. Rice, "Silica-clad crystalline germanium core optical fibers," *Opt. Lett.*, vol. 36, p. 687, 2011.
[14] B. L. Scott and G. R. Pickrell, "Silicon optical fiber diameter dependent grain size," *J. J. Cryst. Growth*, vol. 371, p. 134, 2013.
[15] L. Yin and G. Agrawal, "Impact of two-photon absorption on self-phase modulation in silicon waveguides," *Opt. Lett.*, vol. 32, p. 2031, 2007.
[16] J. Leuthold, C. Koos, and W. Freude, "Nonlinear silicon photonics," *Nat. Photonics*, vol. 4, p. 535, 2010.
[17] P. Mehta, N. Healy, N. F. Baril, P. J. A. Sazio, J. V. Badding, and A. C. Peacock, "Nonlinear transmission properties of hydrogenated amorphous silicon core optical fibers," *Opt. Express*, vol. 18, p. 16826, 2010.
[18] K. Narayanan and S. F. Preble, "Broadband all-optical modulation in hydrogenated-amorphous silicon waveguides," *Opt. Express*, vol. 18, p. 8998, 2010.
[19] L. Shen, N. Healy, P. Mehta, T. D. Day, J. R. Sparks, J. V. Badding, and A. C. Peacock, "Nonlinear transmission properties of hydrogenated amorphous silicon core fibers towards the mid-infrared regime," *Opt. Express*, vol. 21, p. 13075, 2013.
[20] C. Grillet, L. Carletti, C. Monat, P. Grosse, B. B. Bakir, S. Menezo, J. M. Fedeli, and D. J. Moss, "Amorphous silicon nanowires combining high nonlinearity, FOM and optical stability," *Opt. Express*, vol. 20, p. 22609, 2012.
[21] P. Mehta, N. Healy, J. R. Sparks, T. D. Day, P. J. A. Sazio, J. V. Badding, and A. C. Peacock, "All-optical modulation using two-photon absorption in silicon core optical fibers," *Opt. Express*, vol. 19, p. 19078, 2011.
[22] P. Mehta, N. Healy, T. D. Day, J. V. Badding, and A. C. Peacock, "Ultrafast wavelength conversion via cross-phase modulation in hydrogenated amorphous silicon optical fibers," *Opt. Express*, vol. 20, p. 26110, 2012.
[23] L. Shen, N. Healy, L. Xu, H. Y. Cheng, T. D. Day, J. H. V. Price, J. V. Badding, and A. C. Peacock, "Four-wave mixing and octave-spanning supercontinuum generation in a small core hydrogenated amorphous silicon fiber pumped in the mid-infrared," *Opt. Lett.*, vol. 39, p. 5721, 2014.
[24] G. P. Agrawal, *Fiber-Optic Communication Systems, 4th Edition*. Wiley, 2010.
[25] G. Genty, S. Coen, and J. M. Dudley, "Fiber supercontinuum sources," *J. Opt. Soc. Am. B*, vol. 24, p. 1771, 2007.
[26] L. Yin, Q. Lin, and G. P. Agrawal, "Soliton fission and supercontinuum generation in silicon waveguides," *Opt. Lett.*, vol. 32, p. 391, 2007.
[27] F. H. Suhailin, L. Shen, N. Healy, L. Xiao, M. Jones, T. Hawkins, J. Ballato, U. J. Gibson, and A. C. Peacock, "Tapered polysilicon core fibers for nonlinear photonics," *Opt. Lett.*, vol. 41, p. 1360, 2016.
[28] C. McMillen, G. Brambilla, S. Morris, T. Hawkins, P. Foy, N. Broderick, E. Koukharenko, R. Rice, and J. Ballato, "On crystallographic orientation in crystal core optical fibers ii: Effects of tapering," *Opt. Mat.*, vol. 35, p. 93, 2012.
[29] Y. Franz, A. F. J. Runge, N. H. H. Ren, K. Ignatyev, M. Jones, T. Hawkins, J. Ballato, U. J. Gibson, and A. C. Peacock, "Material properties of tapered crystalline silicon core fibers," *Opt. Mat. Express*, vol. 7, p. 2055, 2017.
[30] A. D. Bristow, N. Rotenberg, and H. M. van Driel, "Two-photon absorption and kerr coefficients of silicon for $850-2200$ nm," *Appl. Phys. Lett.*, vol. 90, p. 191104, 2007.
[31] N. Healy, J. R. Sparks, M. N. Petrovich, P. J. A. Sazio, J. V. Badding, and A. C. Peacock, "Large mode area silicon microstructured fiber with robust dual mode guidance," *Opt. Express*, vol. 17, p. 18076, 2009.
[32] J. Chen, Y. Sun, and L. A. Wang, "Reducing splicing loss between a silicon-cored optical fiber and a silica optical fiber," *Photon. Tech. Lett.*, vol. 28, p. 1774, 2016.
[33] V. R. Almeida, R. R. Panepucci, and M. Lipson, "Nanotaper for compact mode conversion," *Opt. Lett.*, vol. 28, p. 1302, 2003.
[34] N. Granzow, M. A. Schmidt, W. Chang, L. Wang, Q. Coulombier, J. Troles, P. Toupin, I. Hartl, K. F. Lee, M. E. Fermann, L. Wondraczek, and P. S. J. Russell, "Mid-infrared supercontinuum generation in as_2s_3-silica "nanospike" step-index waveguide," *Opt. Express*, vol. 21, p. 10969, 2013.
[35] H. Ren, A. F. J. Runge, J. Campling, M. Jones, T. Hawkins, J. Ballato, P. Horak, U. Gibson, and A. C. Peacock, "Silicon fibre nano-spike for robust coupling to silica fibres," *CLEO-Europe*, vol. CK-9.2, 2017.

Michael Shell Biography text here.

John Doe Biography text here.

Jane Doe Biography text here.